Op18 reveals the contribution of nonkinetochore microtubules to the dynamic organization of the vertebrate meiotic spindle

Benjamin R. Houghtaling[a], Ge Yang[b,1,2], Alexandre Matov[b,1], Gaudenz Danuser[b,3], and Tarun M. Kapoor[a,3]

[a]Laboratory of Chemistry and Cell Biology, Rockefeller University, New York, NY 10065; and [b]Laboratory for Computational Cell Biology, Scripps Research Institute, La Jolla, CA 92037

Edited by Don W. Cleveland, University of California at San Diego, La Jolla, CA, and approved July 14, 2009 (received for review March 3, 2009)

Accuracy in chromosome segregation depends on the assembly of a bipolar spindle. Unlike mitotic spindles, which have roughly equal amounts of kinetochore microtubules (kMTs) and nonkinetochore microtubules (non-kMTs), vertebrate meiotic spindles are predominantly comprised of non-kMTs, a large subset of which forms an antiparallel "barrel" array at the spindle equator. Though kMTs are needed to drive chromosome segregation, the contributions of non-kMTs are more mysterious. Here, we show that increasing the concentration of Op18/stathmin, a component of the chromosome-mediated microtubule formation pathway that directly controls microtubule dynamics, can be used to deplete non-kMTs in the vertebrate meiotic spindle assembled in *Xenopus* egg extracts. Under these conditions, kMTs and the spindle pole-associated non-kMT arrays persist in smaller spindles. In excess Op18, distances between sister kinetochores, an indicator of tension across centromeres, remain unchanged, even though kMTs flux poleward with a ≈30% slower velocity, and chromosomes oscillate more than in control metaphase spindles. Remarkably, kinesin-5, a conserved motor protein that can push microtubules apart and is required for the assembly and maintenance of bipolar meiotic spindles, is not needed to maintain spindle bipolarity in the presence of excess Op18. Our data suggest that non-kMTs in meiotic spindles contribute to normal kMT dynamics, stable chromosome positioning, and the establishment of proper spindle size. We propose that without non-kMTs, metaphase meiotic spindles are similar to mammalian mitotic spindles, which balance forces to maintain metaphase spindle organization in the absence of extensive antiparallel microtubule overlap at the spindle equator or a key mitotic kinesin.

stathmin | bipolarity | flux | kinesin-5

Errors in chromosome segregation during meiosis have been linked to developmental defects and abortive pregnancies in humans (reviewed in ref. 1). Accuracy in meiosis depends upon proper attachments of each chromosome to microtubules in a bipolar spindle. The assembly of the bipolar spindle involves complex regulation of the polymerization dynamics and positioning of microtubules. Extensive research into the properties of spindle microtubules has led to their classification into (*i*) kinetochore microtubules (kMTs), which directly interact with kinetochores, and (*ii*) nonkinetochore microtubules (non-kMTs), which interact with chromosome arms and other microtubules, including those with opposite polarity at the spindle equator (reviewed in ref. 2). In vertebrate meiotic spindles, non-kMTs comprise ≈95% of the spindle microtubules (3). These non-kMTs can organize into bipolar spindles in the absence of kinetochores and centrosomes (4). However, many questions persist regarding the coupling between the properties and functions of non-kMTs and kMTs. In particular, it is not known if non-kMTs are needed for kMTs to generate force or to maintain spindle bipolarity.

The continuous poleward translocation of the microtubule lattice, termed poleward flux, is a property of spindle microtubules conserved in higher eukaryotes (reviewed in refs. 5–7). Quantitative fluorescent speckle microscopy (qFSM; reviewed in ref. 8) has provided important insights into the dynamic organization of meiotic spindle microtubules. It has been shown that both kMTs and non-kMTs flux poleward, but at different rates (9–12). More recently, it has been shown that microtubule flux rate changes across the length of metaphase meiotic spindle (13). Two velocity modes for poleward flux were revealed by statistical analysis, and led to the proposal that non-kMTs in the spindle can be subdivided into a "barrel" array of antiparallel overlapping microtubules centered on chromosomes, and 2 "polar" arrays of microtubules at each end of the spindle. Single-fluorophore qFSM has allowed the flux of individual microtubules in meiotic spindles to be examined, and the length and spatial distribution of microtubules to be estimated (14). Together, these recent FSM studies suggest that the vertebrate meiotic spindle is comprised mostly of microtubules that are shorter than half the length of the spindle, and are organized into a barrel array that is dynamically coupled to the 2 polar arrays. Perturbations that can selectively disrupt barrel or polar microtubule arrays are needed to examine how they contribute to kMT function and spindle bipolarity.

Spindle microtubule formation depends on different pathways, including chromatin-mediated and centrosome-mediated formation (reviewed in ref. 15). The barrel and polar array organization was observed in meiotic spindles assembled in the absence of centrosomes (13), indicating that disrupting centrosome-mediated microtubule formation would not be useful in dissecting the contributions of these 2 subsets of spindle microtubules. The GTPase Ran and the kinase Aurora B are involved in chromosome-mediated microtubule formation in vertebrate meiosis. In current models, Ran-GTP binds to importins and thereby releases a wide range of proteins involved in spindle assembly (reviewed in refs. 15 and 16). Aurora B has been proposed to act independently of the Ran pathway (17) and, currently, is believed to have a smaller subset of substrates whose phosphorylation directly controls microtubule stability. These include MCAK (18–20), a kinesin-13 that can catalyze microtubule disassembly (reviewed in ref. 21), and Op18/stathmin (herein referred to as Op18) (17, 22), a microtubule destabilizing protein that binds to tubulin dimers and can promote microtubule catastrophe in vitro (reviewed in ref. 23). We reasoned that controlled perturbations of MCAK or Op18 may allow us to selectively impair the barrel array of non-kMTs.

Author contributions: B.R.H. and T.M.K. designed research; B.R.H. performed research; A.M. and G.D. contributed new reagents/analytic tools; B.R.H., G.Y., A.M., and G.D. analyzed data; and B.R.H. and T.M.K. wrote the paper.

The authors declare no conflict of interest.

This article is a PNAS Direct Submission.

[1]G.Y. and A.M. contributed equally to this work.

[2]Present address: Lane Center for Computational Biology and Department of Biomedical Engineering, Carnegie Mellon University, Pittsburgh, PA 15213.

[3]To whom correspondence may be addressed. E-mail: gdanuser@scripps.edu or kapoor@rockefeller.edu.

This article contains supporting information online at www.pnas.org/cgi/content/full/0902317106/DCSupplemental.

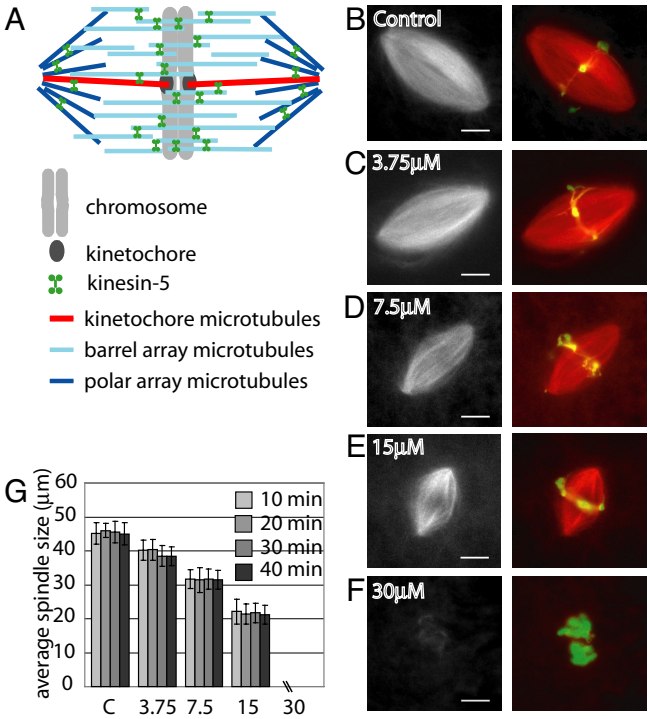

Fig. 1. Increasing Op18 concentration decreases spindle length. (*A*) Proposed barrel model for the meiotic spindle (13). (*B–F*) Spindles formed in *Xenopus laevis* egg extract were labeled with 0.2 μM X-rhodamine tubulin and treated with either buffer alone or the indicated concentration of excess recombinant Op18. Following a 15-min incubation after addition of Op18, spindles were fixed and imaged. (*Left*) Widefield images of labeled tubulin. (Right) Merged images of labeled tubulin (red) and DNA (green). (*G*) Bar graph reporting the average spindle length of fixed spindles, measured as pole-to-pole distance, at indicated time points and concentrations of recombinant Op18. N = >60 spindles for each time point. Error bars represent one standard deviation. (Scale bar: 10 μm.)

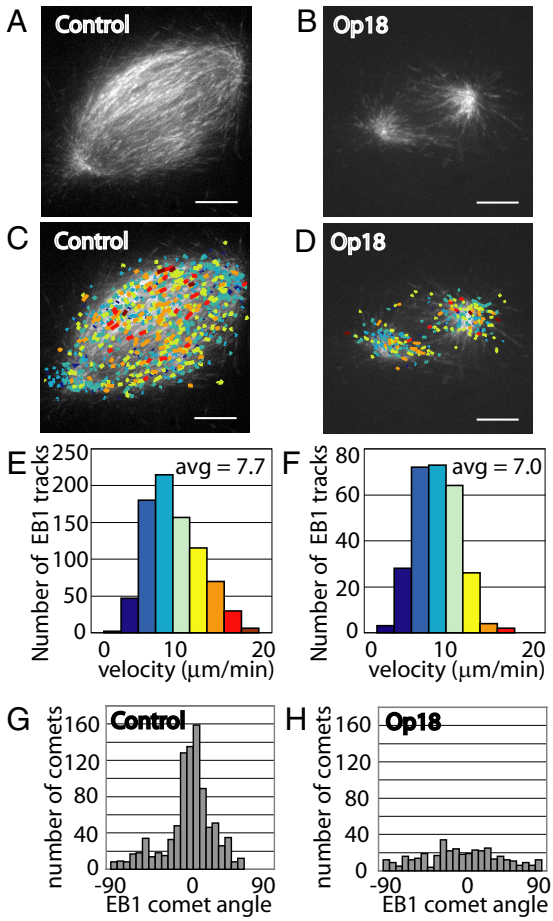

Fig. 2. Microtubule polymerization rates are not affected upon treatment with 15 μM Op18. (*A*) Control spindle labeled with 0.013 mg/mL (≈0.5 μM) Alexa^{488}-labeled recombinant EB1, imaged by confocal microscopy. (*B*) Spindle treated with 15 μM Op18, labeled with Alexa^{488}-EB1, and imaged as in panel *A*. (*C*) EB1 comets from time-lapse sequence of control spindle in panel *A* were detected and tracked using automated software. Tracks were colored to reflect velocity, with blue colors being slower than red colors (see histogram in Fig. 2*E*). Colored EB1 tracks were overlaid onto a single frame from the control spindle time-lapse. (*D*) EB1 comet tracking was performed as in panel *C* for the Op18-treated spindle, and EB1 were tracks overlaid onto a single EB1 frame. (*E*) Histogram of EB1 track velocities detected in the control spindle. Average EB1 track velocity for the control spindle shown = 7.7 μm/min, average velocity of multiple control spindles = 8.0 μm/min (n = 6). (*F*) Histogram of EB1 track velocities detected in spindle treated with 15 μM Op18. Average EB1 track velocity for the Op18-treated spindle shown = 7.0 μm/min, average velocity of multple Op18 treated spindles = 7.3 μm/min (n = 4). (*G*) Angle distribution histogram for EB1 comets detected in *C*. (*H*) Angle distribution histogram for EB1 comets detected in *D*. (Scale bar: 10 μm.)

Results

To deplete the barrel array of microtubules in the meiotic spindle (Fig. 1*A*), we examined the effect of adding excess MCAK or Op18 to spindles formed in *Xenopus laevis* egg extract. Bipolar spindle size was reduced upon addition of excess recombinant human MCAK (supporting information (SI) Fig. S1 *A* and *B*), consistent with previous reports (3). However, excess MCAK also resulted in a significant increase in abnormal spindle structures (Fig. S1 *C* and *D*) (3). The addition of excess Op18 also reduced spindle size, as reported previously (24, 25). We observed a dose-dependent decrease in spindle size upon addition of up to 2.5-fold excess Op18 (endogenous Op18 concentration of 6 μM [26], 15 μM of recombinant Op18 added) (Fig. 1 *B–E*). At higher Op18 concentrations, spindle structures were rarely observed (Fig. 1*F*). The observed smaller spindles maintained size and shape over several minutes, indicating that these structures were at steady state, and not intermediates that would eventually collapse (Fig. 1*G*). Because more reliable control over spindle size could be achieved by adding excess Op18, we used this reagent in further experiments. Though smaller spindles were observed when excess Op18 was added either before or after spindle assembly (Fig. 1 and Fig. S2*A* and *B*), the remaining data presented here was obtained by the addition of excess Op18 to preformed spindles.

To examine the distribution and polymerization of dynamic microtubules upon addition of excess Op18, we used fluorescent EB1, a reporter that binds to the plus ends of growing microtubules (27), and quantitative computer-based tracking. In control spindles, a dense distribution of EB1 traces, or comets, was present throughout the spindle (Fig. 2*A* and Movie S1). Upon addition of 15 μM recombinant Op18, EB1 comets continued to emanate from the spindle poles, but rarely reached past the spindle equator (Fig. 2*B* and Movie S2). A striking feature of the dynamic imaging was that EB1 comets were greatly diminished near the spindle equator, indicating a decrease in growing microtubules in this region. Automated detection and tracking of EB1 comets in control spindles and spindles treated with 2.5-fold excess Op18 revealed similar rates of growth in both spindles types, with an average velocity of 8.0 μm/min in control spindles (n = 6 spindles, SD = 0.93 μm/min, 6,295 total tracks) and 7.3 μm/min in Op18-treated spindles (n = 4 spindles, SD = 0.40 μm/min, 1,313 total tracks). Fig. 2 *C* and *E* reflect data from one control spindle shown in Fig. 2*A*; Fig. 2 *D* and *F* reflect data from one spindle treated with excess Op18, shown in Fig. 2*B*. These data suggest that 2.5-fold increases

CELL BIOLOGY

in Op18 concentration reduce spindle size without significantly reducing polymerization rates of the microtubule filaments in these spindles. Qualitatively, these data also suggest that the non-kMT barrel array may be depleted in the spindles treated with excess Op18, whereas polar non-kMTs and kMTs persist.

We conducted 3 additional analyses to examine if increases in Op18 concentration led to the selective depletion of the barrel array of non-kMTs. First, we examined the orientation of EB1 comets, as the angle of microtubule growth can be used to examine where the microtubule filament may have formed in the spindle. Individual EB1 comets were detected and scored as an angle relative to the pole-to-pole axis of the spindle. In control spindles, EB1 comets distributed over a wide range of angles, with a significant peak at an angle parallel to the pole-to-pole axis, i.e., 0° (Fig. 2*G*). This pattern reflects comets emanating from the poles in all directions, with the predominant angle reflecting the large number of comets in the spindle equator that are parallel to the pole-to-pole axis and are the filaments that form the barrel array of microtubules. In spindles treated with 2.5-fold excess Op18, EB1 comets at all angles were detected; however, no substantial peak was observed at 0° (Fig. 2*H*), indicating that microtubules continued to emanate from each spindle pole in all directions, but the filaments parallel to the pole-to-pole axis were reduced substantially.

As a second test, we examined antiparallel overlap in the spindle. Non-kMTs in the barrel array are thought to establish antiparallel overlap at the spindle equator. One measure of this antiparallel overlap is the detection of microtubule flux toward the distal pole within each half spindle. Most of the microtubules within a half spindle flux poleward. However, a subset of the microtubules, particularly nearer to the equator, move toward the opposite pole, generally associated with antiparallel filament sliding. We used qFSM to analyze this aspect of spindle microtubule organization. Each spindle was divided into halves, and fluorescent tubulin speckle tracks moving toward one pole within the half, or the opposite pole, were counted. In control spindles, an average of 18% of microtubules in each half of the spindle translocated toward the distal pole (Fig. S3 *A–C* and *G*, Movie S3), reporting on the extent of antiparallel overlap of spindle microtubules. In contrast, in Op18-treated spindles, 3.8% of microtubules in each half spindle translocated toward the distal pole (Fig. S3 *D–G* and Movie S4). This remaining fraction of speckles detected that move toward the distal pole upon treatment with Op18 may represent either a few remaining barrel array microtubules, the minor frequency of automated tracking errors, or short microtubule filaments that have yet to properly orient within the spindle.

As a third test of the selective depletion of barrel array non-kMTs, we examined kMTs in bipolar spindles formed in the presence of increased levels of Op18. Chromosomes in spindles treated with excess Op18 are aligned (Fig. 1), suggesting that kMTs remain. To examine kMTs in spindles treated with 2.5-fold excess Op18, we used dual-mode confocal microscopy. In control spindles, several kinetochore pairs, detected using a fluorescent antibody for the inner kinetochore protein CENP-A (10), were present within a dense array of microtubules in a single focal plane (Fig. 3 *A* and *C* and Movie S5). As expected, many microtubules traversed the spindle equator without any apparent association with kinetochores. In contrast to control spindles, essentially all microtubules at the equator of the smaller Op18-treated spindles were positioned such that bundles ended at CENP-A markers (Fig. 3 *B* and *D*). Time-lapse sequences confirmed that these microtubule bundles moved and changed lengths as the kinetochores oscillated, consistent with these bundles representing kinetochore fibers (Movie S6). In support of the depletion of barrel non-kMTs and retention of kMTs, line scans across the spindle equator for both the fluorescent CENP-A and fluorescent tubulin channel were performed. Tubulin intensity in control spindles correlated weakly with kinetochore intensity, reflected in a correlation coefficient of 0.23 (Fig. 3*E*). In contrast, tubulin intensities in Op18-treated spindles strongly correlated with kinetochore intensities, yielding a correlation coefficient of 0.67 (Fig. 3*F*). Together, these data suggest that a 2.5-fold excess of Op18 selectively depletes barrel microtubules at the center of the spindle, leaving kMTs and the 2 polar arrays of non-kMTs. Therefore, we selected this Op18 concentration to examine the contributions of the barrel array of non-kMTs to kMT function and maintenance of spindle bipolarity.

Interkinetochore stretching is one readout of the forces generated by the spindle on single chromosomes (28). We labeled kinetochores using the fluorescent CENP-A antibody (Fig. 3*G*) and treated with 15 μM recombinant Op18 (Fig. 3*H*) or 10 μM nocodazole to disassemble spindles and lose tension (Fig. 3*I*), and compared the interkinetochore distance to that observed in untreated meiotic spindles. In control spindles the kinetochore pair separation was found to be 1.15 μm (SD = 0.11 μm, n = 8 spindles, 55 kinetochore pairs), similar to reported values (10). In Op18-treated spindles the average interkinetochore distance was 1.15 μm (SD = 0.10 μm, n = 11 spindles, 68 kinetochore pairs), whereas kinetochore separation upon nocodazole treatment was 0.5 μm (SD = 0.06 μm, 12 kinetochore pairs) (Fig. 3*J*). Of note, we observed an increased frequency in the oscillation of kinetochore pairs in the presence of excess Op18 (Fig. 3*K*; cf. Movies S5 and S6). Chromosome oscillations have been the focus of intense research over the years and are proposed to depend on forces acting at kinetochores and chromosomes arms. As interkinetochore distance measurements indicate that the forces acting at kinetochores are similar to those in controls, it is likely that these increased oscillations reflect the changes in forces acting on chromosomes arms (29), mediated by the barrel array of non-kMTs.

The detection of kMTs and normal interkinetochore tension in spindles treated with 2.5-fold excess Op18 raises the possibility that kMTs may continue to flux in the absence of barrel-array non-kMTs. To check if this is the case, we used dual-mode confocal microscopy, imaging tubulin speckles (Fig. 4 *A* and *E*, and Movies S7 and S8), and CENP-A kinetochore marks. Kinetochore marks were used to detect where kMT plus-ends were located. Narrow bands of ≈1.12 μm in width, drawn around detected kinetochores, were juxtaposed onto tubulin time-lapse images for control (Fig. 4*B*) and Op18-treated spindles (Fig. 4*F*). Speckles in these regions were detected and tracked using qFSM software (Fig. 4 *C* and *D* reflect tracking data from one control spindle [Fig. 4*A*] and Fig. 4*G* and *H* reflect tracking data from one Op18-treated spindle [Fig. 4*E*]). In control spindles, average speckle velocity in kinetochore regions was 2.09 μm/min (n = 5 spindles, 331 total tracks, SD of average spindle velocity = 0.08 μm/min). In spindles treated with 2.5-fold excess Op18, kinetochore proximal regions had an average speckle velocity of 1.42 μm/min (n = 12 spindles, 513 total tracks, SD of average spindle velocity = 0.22 μm/min). These data suggest that the reduction in kMT flux may be due to a direct effect of excess Op18, or the result of loss of coupling between kMT and barrel-array non-kMTs (discussed in more detail hereafter).

We also examined flux rates in the whole spindle under control and Op18-treated conditions, and found a ≈30% decrease in flux rate (average control spindle flux = 2.03 μm/min, average Op18-treated spindle flux = 1.36 μm/min; Fig. S4). Recent work examining regional variation in flux in metaphase spindles assembled in *Xenopus* egg extracts indicated that there are 2 modes of flux (≈2.7 and ≈1.9 μm/min) likely corresponding to 2 distinct flux-driving mechanisms, with the faster flux associated with the barrel array of non-kMTs and the slower flux with the 2 polar arrays of non-kMTs (13). Interestingly, the overall flux rate we see in spindles treated with excess Op18 is similar, relative to control rates, to the slower mode of flux, consistent with a spindle lacking the faster fluxing barrel array.

The sliding of antiparallel overlapping barrel non-kMTs by kinesin-5 is proposed to be responsible for formation and maintenance of spindle bipolarity (30). However, the observed reduction in barrel array microtubules in spindles treated with 2.5-fold excess

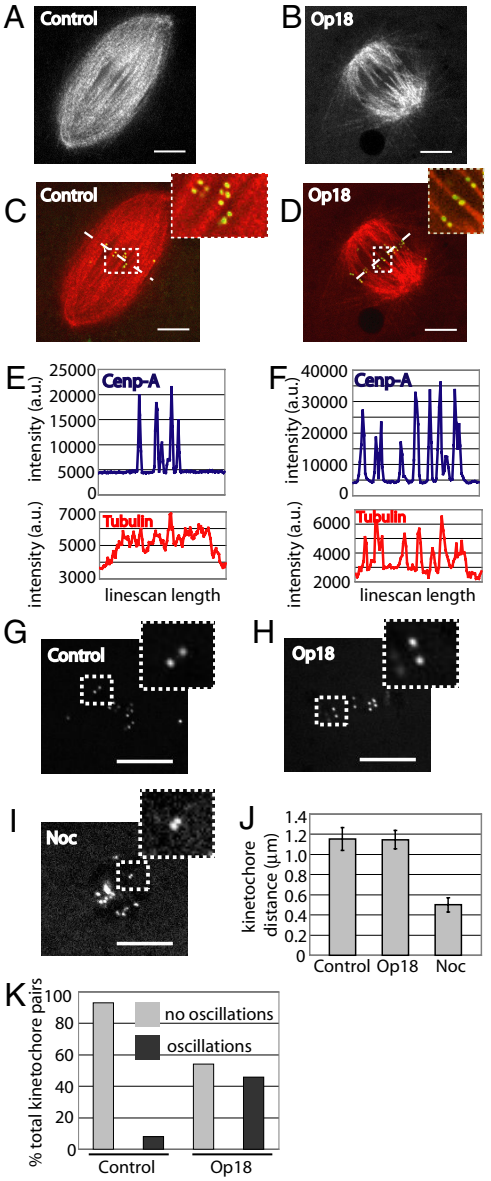

Fig. 3. Kinetochore microtubules persist and interkinetochore tension is maintained in spindles treated with excess Op18. (*A*) Control spindle labeled with 75 nM X-rhodamine tubulin, imaged in a single focal plane by confocal microscopy. (*B*) A 15 μM Op18-treated spindle, labeled and imaged as in panel *A*. (*C*) Merge of tubulin image (red) from control spindle (*A*) with Alexa^{488}-conjugated CENP-A kinetochore marker antibody (green). Dashed box indicates region magnified in the upper right. Dashed line represents position of line for line scan in panel *E*. (*D*) Merge of tubulin image (red) from Op18-treated spindle in panel *D* with Alexa^{488}-conjugated CENP-A kinetochore marker antibody (green). Dashed box indicates region magnified in the upper right. Dashed line represents position of line for line scan in panel *F*. (*E*) Line scan intensities across spindle equator for the CENP-A image and corresponding tubulin image for control spindle in panel *C*. *x* axis represents length of line drawn across the spindle midzone; *y* axis represents arbitrary intensity units. (*F*) Line scan intensities across Op18-treated spindle equator from panel *D* were performed as in panel *E*. (*G–I*) Confocal single plane image of spindle kinetochores, labeled with Alexa^{488}-conjugated CENP-A antibody, and treated with DMSO (*G*), 15 μM Op18 (*H*), or 10 μM nocodazole (*I*). White dashed box indicates magnified region. (*J*) Bar graph of the average distance between kinetochore pairs in control and Op18-treated spindles, and nocodazole-treated extract. Error bars represent one standard deviation. (*K*) Kinetochore oscillations were scored in control and Op18-treated spindles. Only kinetochore pairs present for 10 frames or greater (40 sec) were scored, with oscillations being defined as a 2 pixel (0.32 μm) or greater change in distance over total image time. $n = 32$ control spindles (115 kinetochore pairs; 93% no oscillations, 7% oscillations) and 30 Op18-treated spindles (96 kinetochore pairs; 54.2% no oscillations, 45.8% oscillations). (Scale bar: 10 μm.)

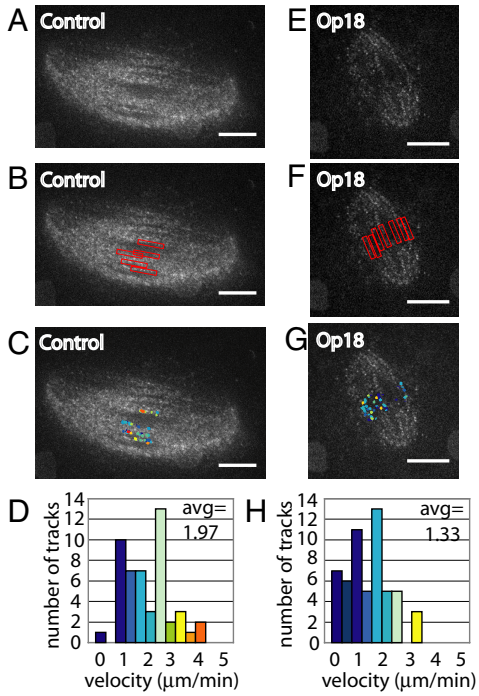

Fig. 4. Kinetochore microtubules flux in spindles lacking barrel-array microtubules. (*A*) Confocal single image of 9.6 nM X-rhodamine tubulin in control spindle. (*B*) CENP-A kinetochore marks were used to manually place restricted analysis regions, indicated by red boxes (≈1.12 μm in diameter), onto time-lapse tubulin speckle images to track kinetochore microtubule flux. (*C*) Speckle tracks detected within the regions defined in panel *B* were overlaid onto a single-frame image of X-rhodamine tubulin. Track colors reflect velocity, as shown in panel *D*. (*D*) Histogram of track velocities detected in control spindle. Average speckle velocity for the control spindle shown = 1.97 μm/min, average speckle velocity of multiple control spindles = 2.09 μm/min ($n = 5$). (*E–G*) Same as panels *A–C*, conducted on a spindle treated with 15 μM Op18. (*H*) Histogram of track velocities detected in spindle treated with 15 μM Op18. Average speckle velocity for the Op18-treated spindle shown = 1.33 μm/min, average speckle velocity of multiple Op18 treated spindles = 1.42 μm/min ($n = 12$). (Scale bar: 10 μm.)

Op18 indicated that kinesin-5 activity may not be required for spindle bipolarity. First, we examined spindle formation in the presence of both the kinesin-5 inhibitor monastrol and excess Op18. The resulting monopolar structures confirmed the requirement for kinesin-5 in spindle formation (Fig. S2). Next, we tested the requirement for kinesin-5 in maintenance of bipolarity in spindles treated with Op18. To do this, monastrol (100 μM) was added to control (Fig. 5*A*) and 2.5-fold excess Op18-treated spindles (Fig. 5*C*). Control spindles treated with monastrol collapsed into monopolar structures within 30 min, as reported previously (31) (Fig. 5*B*). In contrast, Op18-treated spindles maintained bipolarity in the presence of 100 μM monastrol (Fig. 5 *D* and *E*). Similar experiments were conducted with a second kinesin-5 inhibitor, S-trityl-L-cysteine (STLC), yielding identical results (Fig. S5).

The maintenance of bipolarity upon inhibition of kinesin-5 allowed us to examine the contribution of kinesin-5 to poleward flux in spindles depleted of barrel-array non-kMTs. To test this, we used qFSM to measure flux rates in spindles treated with Op18 and monastrol. The average flux rate in spindles treated with 100 μM monastrol and 15 μM Op18 was 1.31 μm/min ($n = 10$ spindles, SD = 0.13 μm/min), similar to rates measured in spindles treated with Op18 alone, indicating that kinesin-5 is not contributing significantly to flux in spindles treated with Op18 alone (Fig. 5*F*, Fig. S4, and Movie S9). Together, these data indicate that the smaller spindles observed in the presence of excess Op18, consisting of kMTs and polar-array microtubules, maintain bipolarity and a

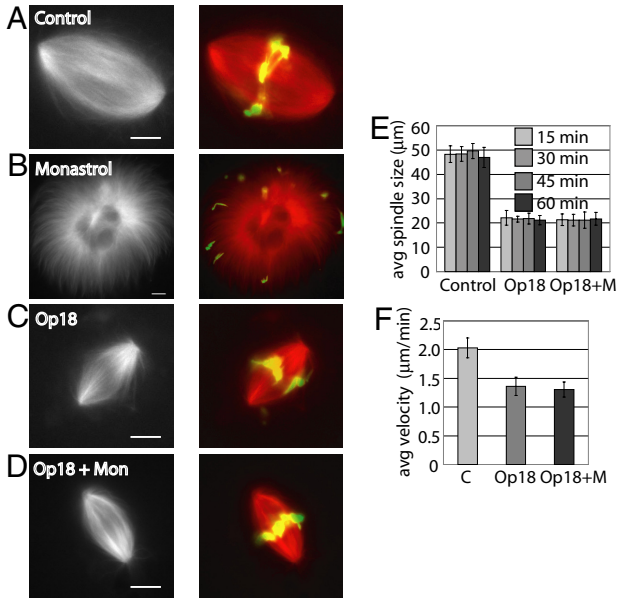

Fig. 5. Spindles depleted of barrel-array microtubules maintain bipolarity upon kinesin-5 inhibition. (*A–D*) Spindles were labeled with 0.2 μM X-rhodamine tubulin and treated with DMSO control (*A*), 100 μM monastrol for 40 min (*B*), 15 μM Op18 for 40 min (*C*), or 15 μM Op18 for 10 min, followed by 100 μM monastrol for 30 min (*D*). Widefield images of labeled tubulin in black and white (*Left*). Merged widefield images of tubulin (red) and DNA (green) (*Right*). (*E*) Bar graph of average spindle length, measured as pole-to-pole distance, of fixed spindles at indicated time points treated with DMSO, 15 μM Op18, or 15 μM Op18 and 100 μM monastrol. $N = >30$ spindles for each time point. Error bars represent one standard deviation. (*F*) Bar graph reporting the average velocity of speckles in control spindles (average speckle velocity = 2.03 μm/min, $n = 5$ spindles, SD = 0.17 μm/min), spindles treated with 15 μM Op18 (average speckle velocity = 1.36 μm/min, $n = 12$ spindles, SD = 0.16 μm/min), and spindles treated with 15 μM Op18 and 100 μM monastrol (average speckle velocity = 1.31 μm/min, $n = 10$ spindles, SD = 0.13 μm/min). Error bars represent one standard deviation between average velocities for all spindles in each condition. (Scale bar: 10 μm.)

reduced poleward flux rate independent of kinesin-5 activity and barrel-array microtubules.

Discussion

A recent model of the meiotic spindle has proposed the existence of a central barrel array of non-kMTs, which cross-links and stabilizes 2 polar arrays of non-kMTs (13). Here, we show that controlled increases in Op18 concentrations can selectively deplete the barrel array of non-kMTs, while kMTs and the polar arrays remain largely unaffected. The greater stability of kMTs compared with non-kMTs may be expected as changes in temperature or Ca^{+2} concentrations can be used to deplete non-kMTs while preserving kMTs (32–35). This probably reflects the action of a dedicated set of kMT cross-linking proteins that confer stability. The mechanism of resistance of polar non-kMTs is less clear. Though polymerization rates of polar non-kMTs are not affected by excess Op18 at concentrations that destabilize barrel array non-kMTs, other parameters of microtubule dynamics we did not measure may differ, including minus-end depolymerization rates. It is also possible that the stability of the polar array of non-kMTs depends on different regulatory mechanisms concentrated at the spindle poles, such as the kinase Aurora A and the microtubule-associated protein Tpx2 (reviewed in ref. 36).

Metaphase spindle size is known to depend more on proteins that regulate microtubule dynamics (e.g., XMAP215, EB1, kinesin-8, and kinesin-13) than on the activities of motor proteins that slide filaments (e.g., kinesin-5) (37). Consistent with these findings, we observe a titration-dependent effect on spindle size with the addition of excess Op18. However, we currently lack an antibody that can deplete Op18 to examine if the relationship of spindle size and Op18 concentration is simple, and a decrease in Op18 increases spindle size. Recently it has been shown that meiotic spindle size varies between 2 species of *Xenopus*, and a dose-dependent scaling of size can be revealed in experiments mixing these different extracts (38). It will be important to examine if the scaling is mediated through Op18, or other factors regulating the barrel array of non-kMTs in meiotic spindles.

Currently, there are 2 models explaining the flux of non-kMTs in the meiotic spindle. In the first model, flux involves tight coordination between plus-end polymerization throughout the spindle, sliding, and minus-end depolymerization near the spindle poles (reviewed in ref. 39). In the second model, stochastic polymerization and depolymerization events occurring at the plus end of microtubules contribute to microtubule turnover, with no minus-end depolymerization required for disassembly (40). In this "slide and cluster" model, plus-end polymerization is favored in chromatin proximal regions, antiparallel sliding activity of kinesin-5 moves these filaments poleward, and plus-end depolymerization disassembles the filaments within the spindle. As non-kMTs comprise ≈95% of the microtubules in vertebrate meiotic spindles (3), the data examining flux and supporting these models may not report on how kMTs in meiotic spindles flux. Our findings show that after depletion of the barrel array of non-kMTs, kMTs can flux poleward and stretch centromeres, generating forces comparable to that transduced through kMTs in control spindles. Our data also show that the kMTs flux without antiparallel microtubule overlap and therefore kinesin-5 dependent antiparallel filament sliding, consistent with a model in which kMT flux is driven through polymer assembly near kinetochores and disassembly at poles. However, the flux rate we observed in the presence of excess Op18 was significantly lower than in control spindles. There are a few possible explanations for this observation. First, the reduction in kMT flux may reflect direct, but partial, suppression of the microtubule dynamics within kMTs, when Op18 levels are increased. Second, the reduction in kMT flux may report on the minor contribution of barrel-array filament flux to kMT flux, which is mediated via active and passive microtubule cross-linkers, including kinesin-5. In support of this possibility, we find that the inhibition of kinesin-5 in spindles treated with excess Op18 does not alter flux rate compared with spindles treated with Op18 alone. Thus, we favor this second model, and also note that the kMT flux measured here is in remarkable agreement with flux rates measured in bipolar, pinned spindles after kinesin-5 inhibition (13).

In contrast to meiotic spindles, kMTs predominate in spindles that assemble in somatic cells. Inhibition studies suggest that the assembly of both somatic cell and meiotic spindles requires the activity of kinesin-5 for the separation of spindle poles (30). However, the role of kinesin-5 in maintaining bipolarity appears to be different between mitotic and meiotic spindles. Once assembled, bipolar mitotic spindles do not collapse to monopolar structures upon acute kinesin-5 inhibition (31, 41, 42). In contrast, meiotic spindles require kinesin-5 to maintain bipolarity, and inhibiting this motor after spindles have formed leads to their collapse (31). Our findings suggest that the collapse of control meiotic spindles upon kinesin-5 inhibition is due to a force imbalance in the barrel array of microtubules, leading to destabilization of the polar arrays and their subsequent collapse to a monopolar structure. In contrast, kinesin-5 inhibition in spindles treated with excess Op18, which selectively abrogates barrel microtubules, has no effect on the stability of the 2 separated polar arrays and bioriented kMTs. We conclude that, following spindle formation, the role of kinesin-5 is limited to pushing apart filaments (43), driving the flux in the barrel array of antiparallel microtubules, which in turn can make a minor

contribution toward kMT flux. The exact function of the barrel array of non-kMTs in the meiotic spindles remains to be established; however, it is tempting to speculate that it may provide increased mechanical stability to the structure to achieve proper size. The barrel array must also generate forces that act on chromosome arms, which can counteract forces acting at kinetochores and, in meiotic spindles, suppress metaphase chromosome oscillations. We also propose that without the barrel array of microtubules, the meiotic spindle resembles a mitotic spindle that can maintain bipolarity and generate forces to sustain a metaphase plate of aligned chromosomes without kinesin-5 activity.

Materials and Methods

Reagents. Spindles were assembled in cycled *Xenopus laevis* cytostatic factor-arrested (CSF) extract as previously described (44), at a constant temperature of 17 °C. For live imaging, 4 μL of extract was mounted on a glass slide (coverslip sealed with valap; 1:1:1 vasoline, lanolin, paraffin). For fixed squashes, 1 μL of extract was combined with 3 μL of fix (60% glycerol, 1× MMR, 10% formaldehyde, 1 μg/mL Hoescht). Phosphocellulose-purified tubulin was labeled with X-rhodamine as described (45), and diluted in extract to a final concentration of 0.2 μM for widefield imaging, and 75 or 9.6 nM for confocal/FSM imaging. His-tagged *Xenopus laevis* Op18 (identical to the construct used in ref. 25) and His-tagged EB1 (27) were both expressed in *E. coli*, purified over a nickel column, and dialyzed into XB buffer without calcium (10 mM K-Hepes [pH 7.7], 100 mM KCl, 1 mM $MgCl_2$, 50 mM sucrose). EB1 was labeled with Alexa^{488} fluorophore (Invitrogen) and purified from free label using a PD-10 gel filtration column (GE Healthcare). His-tagged full-length human MCAK containing C-terminal GFP was expressed in *E. coli*, purified over a nickel column and subsequent cation exchange column, and eluted with BRB80 buffer (80 mM K-Pipes [pH 6.8], 1 mM $MgCl_2$, 1 mM EGTA) containing 300 mM KCl (purified by Benjamin Kwok and Jeffrey Kim). Alexa^{488}-conjugated CENP-A antibody (a generous gift from Aaron Straight, Stanford University, Palo Alto, CA) (10) was used in extract at a final dilution of 1:160. Monastrol was synthesized as described previously (31), and nocodazole and S-trityl-L-cysteine (STLC) were purchased from Sigma. Each compound was dissolved in DMSO at 50× the final concentration.

Microscopy. Labeled kinetochore, FSM, and EB1 images were acquired using a Nikon TE2000 microscope (Morrell Instruments), with a 100× objective (Plan Apo, 1.4 NA) equipped with an EMCCD Photometric Cascade 512B camera (Roper Scientific), a spinning-disk confocal head and 488 and 568 nm excitation by argon and krypton ion lasers, respectively (Solamere Inc). For FSM and EB1 imaging, confocal sections were acquired every 2–6 sec. All live-imaging studies were conducted at 17 °C. Fluorescence imaging of fixed spindles was performed using a Zeiss Axioplan2 (Carl Zeiss MicroImaging, Inc.), with a 40× objective (Plan Neo, NA 0.75), equipped with an AxioCam MRm camera (Carl Zeiss MicroImaging, Inc.).

Data Analysis. Image processing, spindle length and kinetochore measurements, and line scans were performed using MetaMorph software (MDS Analytical Technologies). For speckle flow analysis, image alignment, speckle detection, and tracking were performed as in described in ref. 13. To detect EB1 comets and compute their angular orientation, we used an algorithm similar to the scale-invariant feature transform (SIFT), which transforms image data into scale-invariant coordinates relative to local features and is described in ref. 46. The algorithm accounts for the preferential elongation of EB1 comets and is robust against variation in contrast, shape, and noise between individual comets, frames, and movies. After detection, the motion of EB1 comets was followed by the same tracking methods as applied for speckle tracking. All programs, including routines for graphical representation of tracks, were custom written in MATLAB (Mathworks) and C++.

ACKNOWLEDGMENTS. We thank Aaron Straight (Stanford University) for kindly providing the Alexa^{488}-conjugated CENP-A antibody, Hironori Funabiki (Rockefeller University) for providing the His-tagged Op18 expression plasmid, Benjamin Kwok and Jeffrey Kim for providing the GFP-MCAK protein, and members of the Kapoor lab for helpful discussions. Funding was provided by the National Institutes of Health (NIH) Grants R01 GM065933 (to T.M.K.) and U01 GM067230 (to G.D.), and NIH National Research Service Award GM078852 postdoctoral fellowship (to B.R.H.).

1. Hassold T, Hunt P (2001) To err (meiotically) is human: The genesis of human aneuploidy. *Nat Rev Genet* 2(4):280–291.
2. Compton DA (2000) Spindle assembly in animal cells. *Annu Rev Biochem* 69:95–114.
3. Ohi R, Burbank K, Liu Q, Mitchison TJ (2007) Nonredundant functions of Kinesin-13s during meiotic spindle assembly. *Curr Biol* 17(11):953–959.
4. Heald R, et al. (1996) Self-organization of microtubules into bipolar spindles around artificial chromosomes in Xenopus egg extracts. *Nature* 382(6590):420–425.
5. Rogers GC, Rogers SL, Sharp DJ (2005) Spindle microtubules in flux. *J Cell Sci* 118(Pt 6):1105–1116.
6. Kwok BH, Kapoor TM (2007) Microtubule flux: Drivers wanted. *Curr Opin Cell Biol* 19(1):36–42.
7. Mitchison TJ, Salmon ED (2001) Mitosis: A history of division. *Nat Cell Biol* 3(1):E17–E21.
8. Danuser G, Waterman-Storer CM (2006) Quantitative fluorescent speckle microscopy of cytoskeleton dynamics. *Annu Rev Biophys Biomol Struct* 35:361–387.
9. Waterman-Storer CM, Desai A, Bulinski JC, Salmon ED (1998) Fluorescent speckle microscopy, a method to visualize the dynamics of protein assemblies in living cells. *Curr Biol* 8(22):1227–1230.
10. Maddox P, Straight A, Coughlin P, Mitchison TJ, Salmon ED (2003) Direct observation of microtubule dynamics at kinetochores in Xenopus extract spindles: Implications for spindle mechanics. *J Cell Biol* 162(3):377–382.
11. LaFountain JR, Jr, Cohan CS, Siegel AJ, LaFountain DJ (2004) Direct visualization of microtubule flux during metaphase and anaphase in crane-fly spermatocytes. *Mol Biol Cell* 15(12):5724–5732.
12. Vallotton P, Ponti A, Waterman-Storer CM, Salmon ED, Danuser G (2003) Recovery, visualization, and analysis of actin and tubulin polymer flow in live cells: A fluorescent speckle microscopy study. *Biophys J* 85(2):1289–1306.
13. Yang G, Cameron LA, Maddox PS, Salmon ED, Danuser G (2008) Regional variation of microtubule flux reveals microtubule organization in the metaphase meiotic spindle. *J Cell Biol* 182(4):631–639.
14. Yang G, et al. (2007) Architectural dynamics of the meiotic spindle revealed by single-fluorophore imaging. *Nat Cell Biol* 9(11):1233–1242.
15. Walczak CE, Heald R (2008) Mechanisms of mitotic spindle assembly and function. *Int Rev Cytol* 265:111–158.
16. Dasso M (2002) The Ran GTPase: Theme and variations. *Curr Biol* 12(14):R502–R508.
17. Kelly AE, et al. (2007) Chromosomal enrichment and activation of the aurora B pathway are coupled to spatially regulate spindle assembly. *Dev Cell* 12(1):31–43.
18. Andrews PD, et al. (2004) Aurora B regulates MCAK at the mitotic centromere. *Dev Cell* 6(2):253–268.
19. Ohi R, Sapra T, Howard J, Mitchison TJ (2004) Differentiation of cytoplasmic and meiotic spindle assembly MCAK functions by Aurora B-dependent phosphorylation. *Mol Biol Cell* 15(6):2895–2906.
20. Lan W, et al. (2004) Aurora B phosphorylates centromeric MCAK and regulates its localization and microtubule depolymerization activity. *Curr Biol* 14(4):273–286.
21. Moore A, Wordeman L (2004) The mechanism, function and regulation of depolymerizing kinesins during mitosis. *Trends Cell Biol* 14(10):537–546.
22. Gadea BB, Ruderman JV (2006) Aurora B is required for mitotic chromatin-induced phosphorylation of Op18/Stathmin. *Proc Natl Acad Sci USA* 103(12):4493–4498.
23. Cassimeris L (2002) The oncoprotein 18/stathmin family of microtubule destabilizers. *Curr Opin Cell Biol* 14(1):18–24.
24. Andersen SS, et al. (1997) Mitotic chromatin regulates phosphorylation of Stathmin/Op18. *Nature* 389(6651):640–643.
25. Budde PP, Kumagai A, Dunphy WG, Heald R (2001) Regulation of Op18 during spindle assembly in Xenopus egg extracts. *J Cell Biol* 153(1):149–158.
26. Belmont LD, Mitchison TJ (1996) Identification of a protein that interacts with tubulin dimers and increases the catastrophe rate of microtubules. *Cell* 84(4):623–631.
27. Tirnauer JS, Grego S, Salmon ED, Mitchison TJ (2002) EB1-microtubule interactions in Xenopus egg extracts: Role of EB1 in microtubule stabilization and mechanisms of targeting to microtubules. *Mol Biol Cell* 13(10):3614–3626.
28. Waters JC, Mitchison TJ, Rieder CL, Salmon ED (1996) The kinetochore microtubule minus-end disassembly associated with poleward flux produces a force that can do work. *Mol Biol Cell* 7(10):1547–1558.
29. Ke K, Cheng J, Hunt AJ (2009) The distribution of polar ejection forces determines the amplitude of chromosome directional instability. *Curr Biol* 19(10):807–815.
30. Kashina AS, Rogers GC, Scholey JM (1997) The bimC family of kinesins: Essential bipolar mitotic motors driving centrosome separation. *Biochim Biophys Acta* 1357(3):257–271.
31. Kapoor TM, Mayer TU, Coughlin ML, Mitchison TJ (2000) Probing spindle assembly mechanisms with monastrol, a small molecule inhibitor of the mitotic kinesin, Eg5. *J Cell Biol* 150(5):975–988.
32. Brinkley BR, Cartwright J, Jr (1975) Cold-labile and cold-stable microtubules in the mitotic spindle of mammalian cells. *Ann NY Acad Sci* 253:428–439.
33. Salmon ED, Begg DA (1980) Functional implications of cold-stable microtubules in kinetochore fibers of insect spermatocytes during anaphase. *J Cell Biol* 85(3):853–865.
34. Mitchison T, Evans L, Schulze E, Kirschner M (1986) Sites of microtubule assembly and disassembly in the mitotic spindle. *Cell* 45(4):515–527.
35. Rieder CL (1981) The structure of the cold-stable kinetochore fiber in metaphase PtK1 cells. *Chromosoma* 84(1):145–158.
36. Kufer TA, Nigg EA, Sillje HH (2003) Regulation of Aurora-A kinase on the mitotic spindle. *Chromosoma* 112(4):159–163.
37. Goshima G, Wollman R, Stuurman N, Scholey JM, Vale RD (2005) Length control of the metaphase spindle. *Curr Biol* 15(22):1979–1988.
38. Brown KS, et al. (2007) Xenopus tropicalis egg extracts provide insight into scaling of the mitotic spindle. *J Cell Biol* 176(6):765–770.
39. Mitchison TJ (2005) Mechanism and function of poleward flux in Xenopus extract meiotic spindles. *Philos Trans R Soc Lond B Biol Sci* 360(1455):623–629.
40. Burbank KS, Mitchison TJ, Fisher DS (2007) Slide-and-cluster models for spindle assembly. *Curr Biol* 17(16):1373–1383.
41. Cameron LA, et al. (2006) Kinesin 5-independent poleward flux of kinetochore microtubules in PtK1 cells. *J Cell Biol* 173(2):173–179.
42. Blangy A, et al. (1995) Phosphorylation by p34cdc2 regulates spindle association of human Eg5, a kinesin-related motor essential for bipolar spindle formation in vivo. *Cell* 83(7):1159–1169.
43. Kapitein LC, et al. (2005) The bipolar mitotic kinesin Eg5 moves on both microtubules that it crosslinks. *Nature* 435(7038):114–118.
44. Desai A, Murray A, Mitchison TJ, Walczak CE (1999) The use of Xenopus egg extracts to study mitotic spindle assembly and function in vitro. *Methods Cell Biol* 61:385–412.
45. Hyman A, et al. (1991) Preparation of modified tubulins. *Methods Enzymol* 196:478–485.
46. Gatlin JC, et al. (2009) Spindle fusion requires dynein-mediated sliding of oppositely oriented microtubules. *Curr Biol* 19(4):287–296.